

UC Berkeley

UC Berkeley Previously Published Works

Title

Non-linearity in engineered lead magnesium niobate ($\text{PbMg}_{1/3}\text{Nb}_{2/3}\text{O}_3$) thin films

Permalink

<https://escholarship.org/uc/item/4c92f35d>

Journal

Journal of Applied Physics, 128(19)

ISSN

0021-8979

Authors

Shetty, Smitha
Kim, Jieun
Martin, Lane W
[et al.](#)

Publication Date

2020-11-21

DOI

10.1063/5.0003635

Peer reviewed

Non-linearity in engineered lead magnesium niobate ($\text{PbMg}_{1/3}\text{Nb}_{2/3}\text{O}_3$) thin films

Cite as: J. Appl. Phys. **128**, 194102 (2020); <https://doi.org/10.1063/5.0003635>

Submitted: 03 February 2020 . Accepted: 02 November 2020 . Published Online: 18 November 2020

 **Smitha Shetty**,  **Jieun Kim**,  **Lane W. Martin**, and  **Susan Trolier-McKinstry**



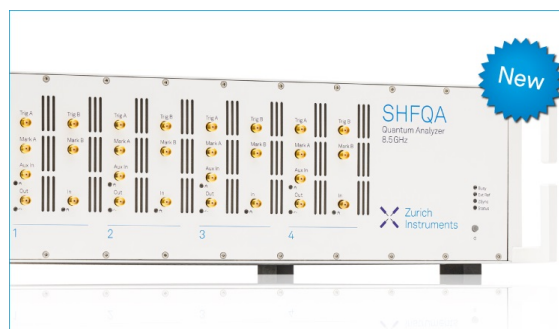
View Online



Export Citation



CrossMark



Your Qubits. Measured.

Meet the next generation of quantum analyzers

- Readout for up to 64 qubits
- Operation at up to 8.5 GHz, mixer-calibration-free
- Signal optimization with minimal latency

Find out more



Non-linearity in engineered lead magnesium niobate ($\text{PbMg}_{1/3}\text{Nb}_{2/3}\text{O}_3$) thin films

Cite as: J. Appl. Phys. **128**, 194102 (2020); doi: 10.1063/5.0003635

Submitted: 3 February 2020 · Accepted: 2 November 2020 ·

Published Online: 18 November 2020



Smitha Shetty,¹ Jieun Kim,² Lane W. Martin,^{2,3} and Susan Trolier-McKinstry¹

AFFILIATIONS

¹Materials Research Institute and Department of Materials Science and Engineering, Pennsylvania State University, University Park, Pennsylvania 16802, USA

²Department of Material Science and Engineering, University of California, Berkeley, 216 Hearst Memorial Mining Building, Berkeley, California 94720, USA

³Materials Sciences Division, Lawrence Berkeley National Laboratory, Berkeley, California 94720, USA

ABSTRACT

The local compositional heterogeneity associated with the lack of long-range ordering of Mg^{2+} and Nb^{5+} in $\text{PbMg}_{1/3}\text{Nb}_{2/3}\text{O}_3$ (PMN) is correlated with its characteristic “relaxor” ferroelectric behavior. Earlier work [Shetty *et al.*, Adv. Funct. Mater. **29**, 1804258 (2019)] examined the relaxor behavior in PMN thin films grown at temperatures below 1073 K by artificially reducing the degree of disorder via synthesis of heterostructures with alternate layers of $\text{Pb}(\text{Mg}_{2/3}\text{Nb}_{1/3})\text{O}_3$ and PbNbO_3 , as suggested by the “random-site model.” This work confirmed the development of ferroelectric domains below 150 K in long-range-ordered films, epitaxially grown on (111) SrTiO_3 substrates using alternate target timed pulsed-laser deposition of $\text{Pb}(\text{Mg}_{2/3}\text{Nb}_{1/3})\text{O}_3$ and PbNbO_3 targets with 20% excess Pb. In this work, the first through third-harmonic dielectric charge displacement densities and complex dielectric susceptibilities were analyzed as a function of temperature and frequency in zero-field-cooled PMN films with short- and long-range ordering. The long-range ordering decreased the dispersion in the first- and third-harmonic dielectric charge displacement densities relative to short-range-ordered films. It was found that the one-dimensional ordering achieved in the long-range-ordered film is insufficient to achieve a fully normal ferroelectric state. In the presence of quenched random electric fields, these films require a small ac field to facilitate percolation of the polar nano-regions, enabling normal ferroelectric-like behavior at lower temperature ($T < 240$ K). The films behave like a typical relaxor near room temperature. With reduced ordering, the short-range films exhibit greater dispersion in linear and higher order harmonic dielectric charge displacement density.

Published under license by AIP Publishing. <https://doi.org/10.1063/5.0003635>

I. INTRODUCTION

Small signal dielectric nonlinearities can be used to probe the response of domain walls^{2–6} or nano-polar regions^{7–10} to oscillating electric fields. This can be a valuable tool in understanding the ferroelectric-relaxor continuum model observed in long-range-ordered $\text{PbMg}_{1/3}\text{Nb}_{2/3}\text{O}_3$ (PMN) films.¹ In materials containing ferroelectric domain walls with a randomly broad and uniform distribution of pinning centers, the polarization response in the sub-switching regime ($E \lesssim 1/2 E_c$, where E_c is the coercive field) may be approximated by the Rayleigh relation:¹¹

$$P = (\epsilon_{init} + \alpha E_0)E \pm \alpha(E^2 - E_0^2) + \dots, \quad (1)$$

where P is polarization, $E = E_0 \sin \omega t$ is the applied alternating electric field, ϵ_{init} is the dielectric permittivity at zero field, and α is the

irreversible Rayleigh coefficient; the “+” sign corresponds to decreasing and “–” to increasing field. The above relationship can be expanded into a Fourier series² as

$$P = (\epsilon_{init} + \alpha E_0)E_0 \sin \omega t - \frac{4\alpha E_0^2}{3\pi} \cos \omega t - \frac{4\alpha E_0^2}{3\pi} \left[\frac{1}{15} \cos 3\omega t - \frac{1}{105} \cos 5\omega t + \dots \right]. \quad (2)$$

In this formulation, the higher harmonic terms are 90° out-of-phase with the driving field; as a result, they contribute both to the nonlinearity in polarization and to hysteresis. This model provides a good description of the response of a number of ferroelectrics^{2,5} with mobile domain walls or boundaries of polar clusters. This field dependence of the phase angle of higher-harmonic

permittivity has been used by Hashemizadeh and Damjanovic to investigate the presence of Rayleigh-like behavior in $\text{Ba}_{0.6}\text{Sr}_{0.4}\text{TiO}_3$ ceramics.¹² In those ceramics, the phase angles were inconsistent with Eq. (2). Instead, the behavior was consonant with harmonic analysis of PMN ceramics above the dielectric maximum temperature (T_{max}), where the polar entities provide a nonlinear, but nearly anhysteretic response¹³ as a function of the electric field, implying that the Rayleigh-like analysis cannot be used to fully explain the dielectric response in this regime.

The non-linear dielectric properties are also important in discriminating between the existing models for relaxor ferroelectrics, since it is believed that the higher order susceptibilities are more sensitive to dipolar disorder than the linear parameters.⁹ In globally centrosymmetric materials like PMN, the dielectric response between induced polarization (P) and the electric field (E) should be given by the following expression:

$$P = \epsilon_0(\chi_1 E + \chi_3 E^3 + \chi_5 E^5 + \dots), \quad (3)$$

where χ_1 and χ_3 are the first- and third-harmonic susceptibilities. There are several conflicting studies on the temperature dependence of the scaled susceptibility parameter χ_3 and a_3 (defined as $a_3 = -\chi_3/\epsilon_0\chi_1^4$) in the vicinity of the static freezing temperature (T_f) of relaxors. Recent work^{14–17} based on the random field model suggests that PMN behaves more like a ferroic glass, such that below Burn's temperature ($T_d \sim 650$ K), the fluctuations in the quenched random electric fields are responsible for the formation and growth of polar nanoregions (PNRs), intermittent glass formation ($T_g \sim 240$ K) followed by percolation into domain-like clusters below 213 K on cooling. In principle, χ_3 and a_3 could distinguish between models in which as a function of ordering, PMN transforms into a ferroelectric state with inhomogeneities^{14,15,17,18} or diverges into a freezing transition, as in the case of a dipolar glass.⁷ Another model for PMN is the spherical random-bond-random-field (SRBRF) model. In the SRBRF model, Pirc and Blinc assumed that spherical PNRs interact via spin-glass-type random exchange coupling, while being subjected to a random quenched internal electric field.^{19,20} The model predicts a negative χ_3 and a positive a_3 with two extremes: one at T_f of the spherical-glass phase and another at T_{max} . To date, this prediction has been examined experimentally by a number of groups^{7,9,21} for PMN single crystals.

TABLE I. Summary of signs for third-harmonic polarization P_3/χ_3 and a_3 and phase for χ_3 predicted by existing models.

Existing models	P_3/χ_3 (sign)	P_3/χ_3 (phase)	a_3 (sign)
Rayleigh model ^{2,12}	P_3 (–)	P_3 (-90°)	+
Modified LGD9-based relaxor model	χ_3 (+)	N/A	–
SRBRF model ¹⁹	χ_3 (–)	180°	+
Generalized SRBRF ²²	χ_3 (+)	180°	–
Ferroic glass model coupled with the presence of ferroelectric domains in PMN at $T < 213$ K ^{14,16}	P_3 (–)	P_3 (-90°)	+

Bobnar *et al.*⁷ confirmed the theoretically predicted anomaly of a_3 at T_f (a_3 strongly increases as the temperature approaches the freezing $T_f \approx 220$ K, where ergodicity is effectively broken for undoped PMN single crystals). Additionally, it was shown that on cooling in a zero electric field, weak relaxors like lanthanum-doped PZT⁷ undergo a transition to a random-bond-driven glass state; the application of an electric field beyond a critical electric field causes a transition into an inhomogeneous random-field-modulated ferroelectric state. However, this phenomenon has not been experimentally demonstrated in PMN. Glazounov and Dec observed that a_3 continues its monotonic increase even below $T_f \approx 220$ K. A monotonic increase in a_3 would be more in agreement with the ferroelectric background picture of relaxors than with the glassy one. The experimental data show a positive sign of χ_3 , which can be explained either by incorporating the effect of the electric field on the interacting polar clusters in the generalized SRBRF model²² or by including the average polarization of the polar nano-regions in a modified Landau–Ginzburg–Devonshire (LGD) formalism.⁹ The signs and phase of third-harmonic polarization or χ_3 and the sign of a_3 are summarized here (Table I) for the Rayleigh model, the modified phenomenological model for relaxors,⁹ the SRBRF model, and the ferroic glass model coupled with the presence of ferroelectric domains at $T < 213$ K.^{14,16} It has been pointed out that many of these seemingly contradictory observations could be due to the fact that the experimental results were obtained in different regions of the electric field–temperature phase diagram.²³ Namely, by cooling the relaxor at an electric field exceeding the critical field E_c , a long-range ferroelectric phase is formed. Thus, the field-history characteristic of the measurement can have a profound effect on the results.

There are essentially two ways to characterize the third-order, non-linear dielectric response χ_3 . The most reliable technique involves the measurement of the polarization response at 3ω , simultaneously with the linear response at ω at zero field dc bias. The second technique utilizes the static electric field dependence of the linear dielectric constant, where χ_3 is defined as

$$\chi_3 = [\chi_1(E_2) - \chi_1(E_1)] / [(E_2)^2 - (E_1)^2]. \quad (4)$$

This method can be erroneous due to contributions from a phase transition into a long-range-ordered ferroelectric state near T_f .

Although symmetry should forbid a second-harmonic-dielectric response in centrosymmetric materials, measurable second-harmonic contributions have been reported for the centrosymmetric phases of paraelectric/relaxor crystals and ceramics like $\text{Ba}_{0.6}\text{Sr}_{0.4}\text{TiO}_3$,¹² PZN-PT,²⁴ BaTiO_3 ,²⁴ $\text{Sr}_{0.61}\text{Ba}_{0.39}\text{Nb}_2\text{O}_6$,²⁵ etc. This has been attributed to the presence of residual polarization. This may be due to the presence of micropolar regions or to a finite defect population, leading to local inhomogeneous fields and quadratic dielectric charge displacement in the material. A second possibility is that a second-harmonic contribution can also be observed in cases where mobile charges are trapped on the first cycle of the electric field.²⁵ Third, the random field model¹⁵ suggests that fluctuations of quenched random electric fields due to charge disorder can give rise to an inhomogeneous field that is responsible for the growth and stabilization of the polar nanoregions. This leads to a net non-zero average polarization in PMN,

thus contributing to χ_2 .⁹ Including the contributions of χ_2 in Eq. (3) for PMN, the Fourier expansion for the net polarization becomes

$$P(t) = \epsilon_0 \chi_1 E_0 \sin \omega t + \frac{\epsilon_0 \chi_1 E_0^2}{2} + \frac{3}{4} \epsilon_0 \chi_3 E_0^3 \sin \omega t - \frac{\epsilon_0 \chi_2 E_0^2}{2} \cos 2\omega t - \frac{\epsilon_0 \chi_3 E_0^3}{4} \sin 3\omega t + \dots \quad (5)$$

It is an open question as to how cation ordering in PMN will affect the higher harmonic polarization terms as a function of temperature. In this work, the first-, second-, and third-harmonic complex dielectric susceptibilities were analyzed as a function of temperature and frequency in zero-field-cooled PMN films with short- and long-range ordering. These, along with the phase angles of the higher harmonics, were used to probe the ferroelectric-relaxor continuum phenomenon. Of particular interest was which, if any, of the models in Table I described the behavior of the PMN films. The measurements also track the nonlinearity over a wider temperature range than has been reported previously.

II. EXPERIMENTAL PROCEDURE

The experimental method for the growth of 100 nm thick long- and 80 nm thick short-range-ordered films via pulsed laser deposition has been described elsewhere.¹ For this study, the short-range-ordered films were grown with a laser fluence of 1.5 J/cm² at a repetition rate of 5 Hz. For the second- and third-order dielectric harmonic measurements, a sinusoidal ac oscillation was applied using the built-in voltage source of a lock-in amplifier (Stanford Research Inc., SR- 830). A low-noise charge amplifier with two different scaling factors of 1 V/113.2 pC and 1 V/22.8 pC, respectively, was used to amplify the output signal of the sample as a function of voltage and temperature. Both the charge amplifiers with a scaling factor showed very little change in amplitude (<2%) and moderate phase errors (<16°) with a reference capacitor load similar to that of the PMN films, at the highest measured frequency of ~70 kHz (e.g., the fifth harmonic of the 14 kHz fundamental). Based on previous work,¹ Rayleigh behavior was found to hold for these films between fields of 15 and 35 kV/cm over a wide temperature range. The resulting voltage from the charge amplifier was detected by the lock-in amplifier for the first through fifth harmonics sequentially. The more sensitive charge amplifier (1 V/22.8 pC) was used at lower temperature and lower applied fields to detect contributions greater than the third harmonic. In this way, the magnitudes and phases of the higher-harmonic dielectric charge displacement densities were measured as a function of temperature and frequency. The harmonic dielectric charge displacement density is defined as $D_n = Q_n/A$, where A is the area of the sample, D_n is the induced dielectric charge displacement density, Q_n is the magnitude of the measured charge at the desired frequency, and n is the harmonic order. The first- and second-harmonic susceptibilities were calculated from D_n using Eq. (5). Since the third-harmonic dielectric charge displacement densities contain contributions from both third- (Q_3) and fifth-harmonic (Q_5) charges, the third-harmonic susceptibility was calculated

using the following relation:

$$\chi_3 = \frac{1}{E_0^3 A \epsilon_0} (-4Q_3 - 20Q_5). \quad (6)$$

As the higher harmonic dielectric charge displacement densities for $n > 5$ were below the measurable threshold for the lock-in amplifier, we have only included contributions up to $n = 5$ in the calculation of higher harmonic susceptibilities at the measured electric field. Similar to the nonlinear dynamic approach adopted by Hashemizadeh *et al.*,¹² the phase of the higher harmonic dielectric measurement was measured separately to investigate the dynamics of the polar mobile interfaces (such as domain walls or polar cluster boundaries), especially to validate the Rayleigh-like behavior regime in the long-range-ordered sample, as a function of temperature and ac fields up to 75 kV/cm at 1 kHz.

III. RESULTS AND DISCUSSION

Figures 1 and 2 show the temperature dependence of the real parts of the first- ($D_{1\omega}'$) and third- ($D_{3\omega}'$) harmonic dielectric charge densities without fifth-harmonic contributions, along with the imaginary part of the second- ($D_{2\omega}''$) harmonic dielectric charge displacement densities for short- and long-range-ordered PMN thin films, respectively, measured at 15 kV/cm. All three responses show broad frequency-dependent maxima as a function of temperature in the frequency range from 0.5 to 14 kHz. $D_{3\omega}'$ is more frequency dependent than $D_{1\omega}'$. As reported previously,¹ the short-range-ordered films show a larger frequency dispersion in $D_{1\omega}'$ compared to the long-range-ordered films. This is consistent with a higher degree of relaxor behavior in the short-range-ordered films.

As seen in Eq. (5), in non-centrosymmetric or polar materials, $D_{2\omega}$ is expected to be 90° out-of-phase with the applied field. Interestingly, the imaginary part ($D_{2\omega}''$) is comparable in both films, with slightly larger magnitude in short-range-ordered films with increased frequency dispersion (similar to $D_{1\omega}'$). Non-zero $D_{2\omega}$ is an indicator of net polarization of the thin film, consistent with that observed in bulk PMN by Dec *et al.*⁹ However, it is interesting to note that in other relaxor systems like BaTi_xZr_xO₃ ceramics,⁸ the increase in chemical and charge disorder causes increased dispersion in χ_1 , with suppression in χ_2 . This has been attributed to instability of the polarization via random field fluctuations.²⁶ However, in PMN, net polarization is assumed to stabilize during the first polarization cycles of the ac susceptibility measurements²⁷ and seems to be unaffected by one-dimensional chemical ordering.

The $D_{3\omega}'$ response has a maximum between 150 and 170 K (observed at the lowest frequencies), with the values converging back toward zero both at 10 K and well above T_{\max} . $D_{3\omega}$ reduces with increasing frequencies in both the long- and short-range-ordered PMN films. The dispersion in $D_{3\omega}$ is small at $T < 100$ K and increases in magnitude with temperature, until it reaches ~150–170 K for both short-range-ordered and long-range-ordered films. Upon further heating, the frequency dispersion collapses. Persistence of larger dispersion up to higher temperature in the short-range-ordered films is consistent with a higher degree of relaxor behavior.

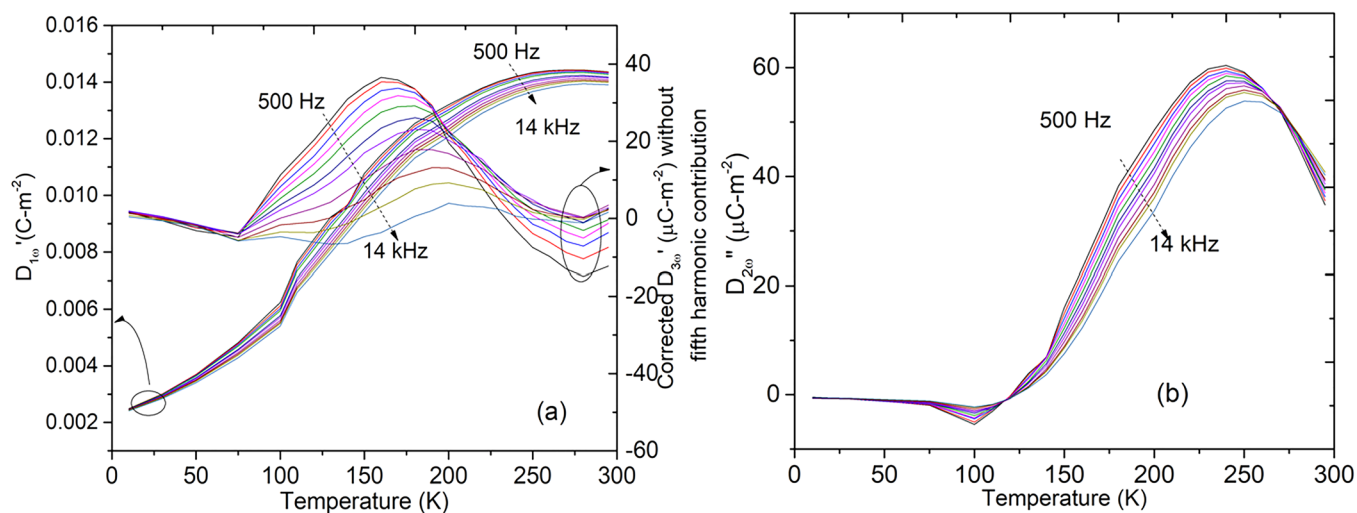


FIG. 1. (a) Temperature dependence of first- and third-harmonic dielectric charge displacement densities for zero-field cooled short-range-ordered PMN films as a function of frequency (500 Hz–14 kHz) measured on heating. (b) Temperature dependence of the imaginary part of second-harmonic dielectric charge displacement density for short-range-ordered PMN films as a function of frequency measured on heating. The dotted arrows indicate increasing frequency (from 500 Hz to 14 kHz). All measurements were done at an electrical field of 15 kV/cm. The Fourier series expansion for $P(t)$ for a polar material only has the imaginary part for second harmonic polarization. $D_{2\omega}$ is expected to be 90° out-of-phase with the applied field, and the real parts are much smaller in magnitude compared to the imaginary parts.

To develop an additional insight into the mechanisms responsible for frequency and ac field dependence, the higher-harmonic polarization was measured as a function of temperature and amplitude of the ac electric field for PMN films with long-range-ordering. Figures 3(a)–3(e) illustrate the phase of the

first- and third-harmonic polarization contributions for long-range-ordered as a function of temperature. At low temperatures, after a certain threshold field, the phase angle of the first harmonic is $\sim 0^\circ$, while that of the third harmonic is -90° , similar to that observed in PZT thin films.² This is consistent with

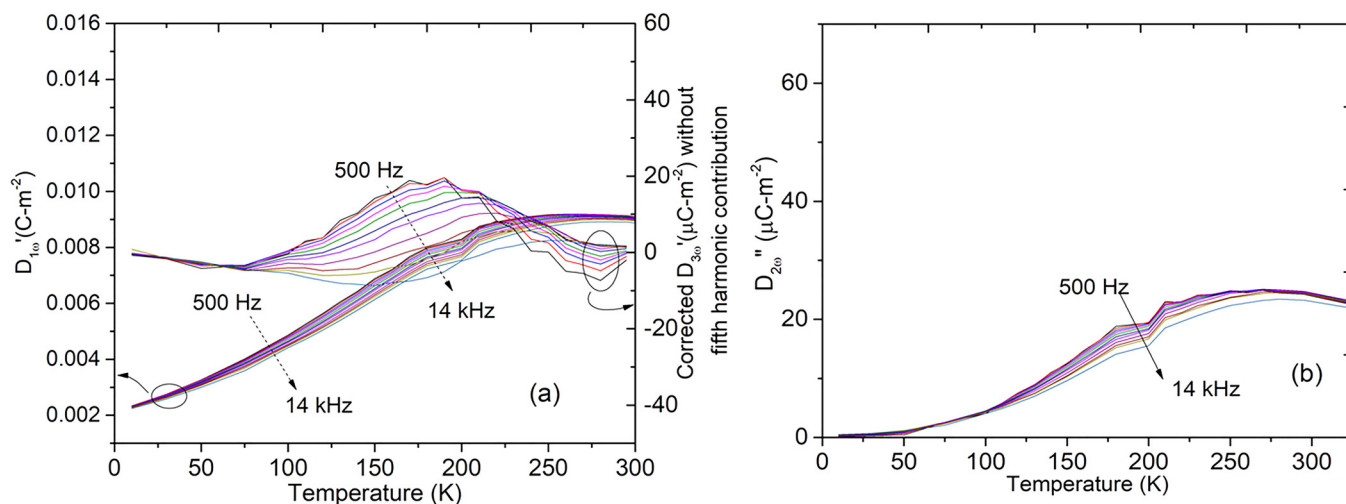


FIG. 2. (a) Temperature dependence of first- and third-harmonic dielectric charge displacement densities for zero-field cooled long-range-ordered PMN films as a function of frequency (500 Hz–14 kHz) measured on heating. (b) Temperature dependence of the imaginary part of the second harmonic dielectric charge displacement density for long-range-ordered PMN films as a function of frequency on heating. The dotted arrows indicate increasing frequency (from 500 Hz to 14 kHz). All measurements were done at an electrical field of 15 kV/cm.

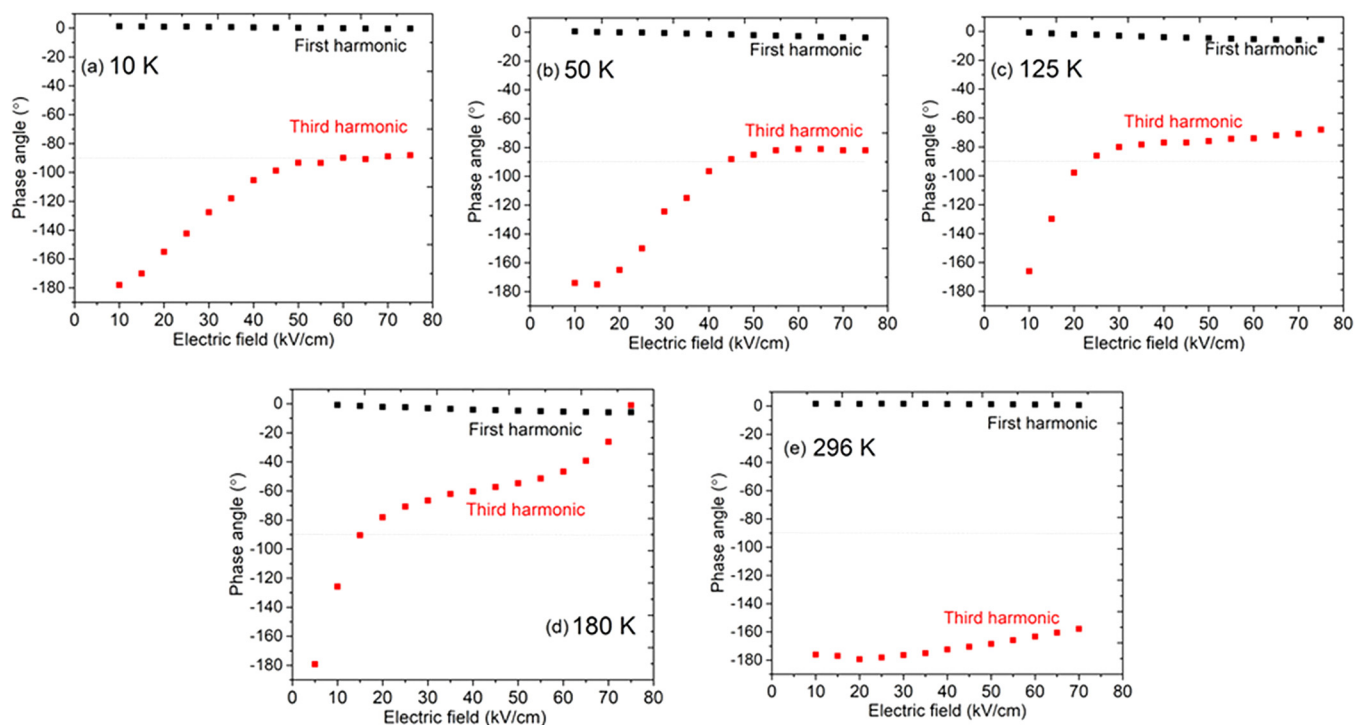


FIG. 3. (a)–(e) Phase angle for the first and the third harmonics of polarization at 10 K, 50 K, 125 K, 180 K, and 296 K demonstrating hysteretic to an-hysteretic transition in long-range-ordered PMN measured at 1 kHz.

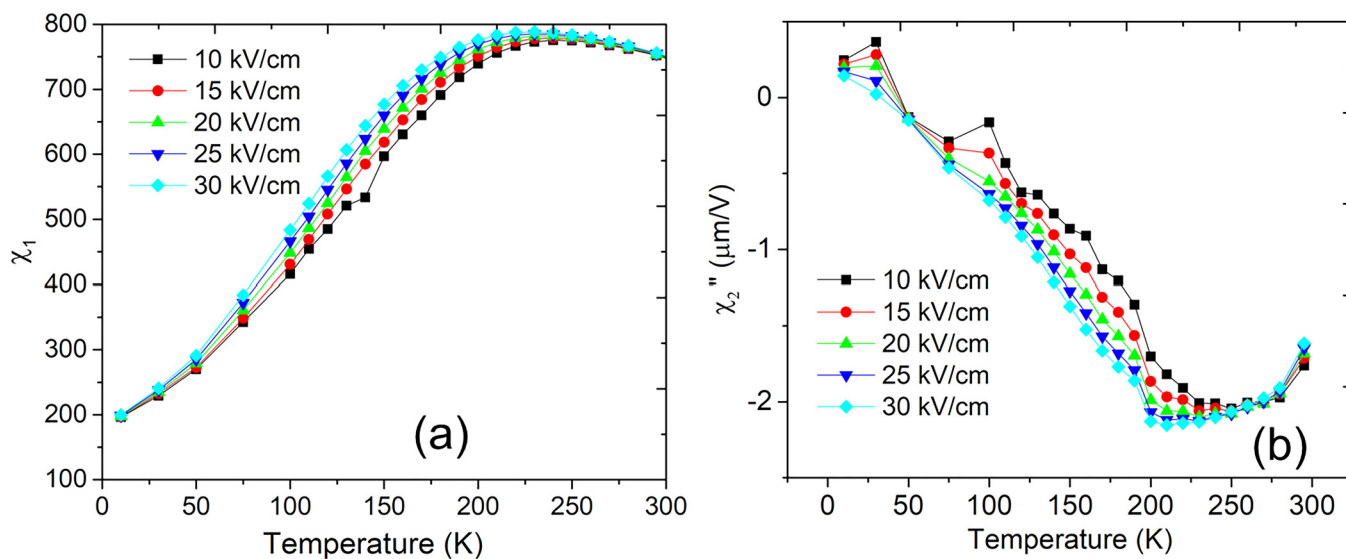


FIG. 4. Temperature dependence of (a) the real part of first- and (b) the imaginary part of second-harmonic susceptibility for long-range-ordered PMN films as a function of electric field (10–30 kV/cm) measured during a heating cycle.

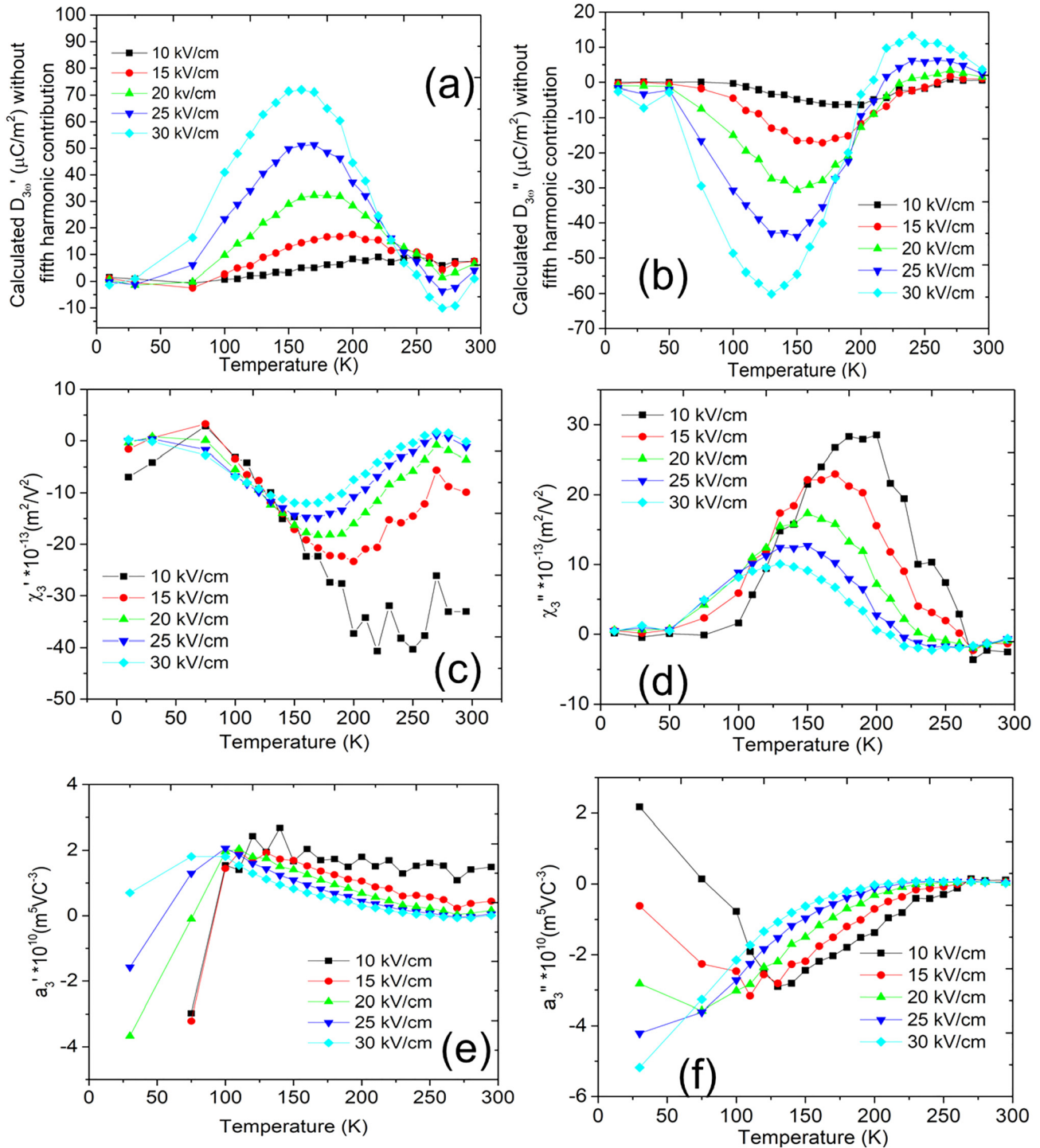


FIG. 5. Temperature dependence of (a) calculated real and (b) calculated imaginary parts of third-harmonic dielectric displacement, (c) real and (d) imaginary parts of third-harmonic susceptibility, (e) scaled-susceptibility parameter a'_3 , and (f) scaled-susceptibility parameter a''_3 for long-range-ordered PMN films as a function of electric field (10–30 kV/cm) measured during a heating cycle. Note the threshold field for the Rayleigh regime (where the phase angle for the third-harmonic lags the applied field by 90°) is greater than 20 kV/cm at temperature less than 210 K.

Rayleigh-like hysteretic responses of mobile interfaces (i.e., domain walls or polar-cluster boundaries).²⁸ The observation of Rayleigh-like behavior at low temperatures is consistent with the drop in the magnitude of $D_{3\omega}$ below 100 K, as the motion of domain walls (or cluster boundaries) is thermally activated. This might also account for the relatively modest frequency dependence, with the largest response occurring at the lowest frequencies.

At temperatures above ~ 180 K, the third-harmonic phase angle deviates away from $\sim 90^\circ$ toward 0° or -180° with increasing field [Figs. 3(d) and 3(e)]. The threshold field (defined as the minimum electric field for observing Rayleigh response where the phase angle is close to 90°) was observed to decrease with increasing temperature. This can provide insight into the energy barrier ranges for domain wall-like motion. This corresponds well with the peak in the irreversible Rayleigh coefficient α at ~ 150 K as reported elsewhere.¹ At room temperature, the third-harmonic angle is close to -180° , representing an-hysteretic behavior similar to that reported in bulk PMN.^{12,13} This means that the dielectric behavior at room temperature is governed by polar nano-regions, whose dynamics cannot be explained using the Rayleigh law. This may occur as a result of increased relaxor behavior due to contributions for the polar nano-region, as proposed by the spherical random bond random field model.¹⁹

Figures 4(a) and 4(b) show the ac field dependence of the real part of first-harmonic (χ_1') and the imaginary part of second-harmonic susceptibility (χ_2'') as a function of temperature measured at 1 kHz for the long-range-ordered PMN thin films. The linear susceptibility displays a broad maximum as a function of temperature. The imaginary part of the second-harmonic susceptibility [Fig. 4(b)] follows a similar trend as linear susceptibility. The magnitude of χ_2'' remains non-zero over the measured temperature range, consistent with the contributions from polar

nano-regions that have been stabilized by the quenched random electric field.

Figures 5(a)–5(f) show the ac field dependence of the real ($D_{3\omega}'$) and imaginary ($D_{3\omega}''$) components of the third-harmonic dielectric charge displacement density without the fifth-harmonic contributions, corresponding real (χ_3') and imaginary parts (χ_3'') of the third-harmonic susceptibility as well as the scaled-parameter a_3' and a_3'' as a function of temperature, measured at 1 kHz for the long-range-ordered PMN thin films. As seen in Fig. 5(a), on cooling, the negative high temperature tail of $D_{3\omega}'$ becomes increasingly positive with the increasing ac field. Corresponding to this, as shown in Fig. 5(c), at the lowest measured field (which is below the threshold field at low temperatures, but well in the Rayleigh regime above ~ 120 K), χ_3' is mostly negative, at temperatures above 100 K. With increasing fields, χ_3' becomes less negative, with its peak shifting to lower temperatures. The negative χ_3' is consistent with the SRBRF model for PMN ceramics.¹⁹ In addition, there is a marked change in sign in the real $D_{3\omega}'$ and imaginary parts of $D_{3\omega}''$ at ~ 240 K as seen in Figs. 5(a) and 5(b) with increasing electric fields. There are two possible mechanisms to explain this change of sign. First, the transition from negative χ_3 (paraelectric state) to positive χ_3 (ferroelectric phase) could indicate a second-order phase transition.¹⁰ However, there is no corresponding peak in χ_1 as might be expected for a relaxor-to-ferroelectric phase transition. Thus, the more likely scenario is the inception of percolation of the polar nanoregions in the long-range-ordered films. The previous results¹ assert that the one-dimensional ordering observed in long-range-ordered PMN heterostructure films is inadequate to drive a fully ferroelectric state. Instead, the mobile boundaries of polar clusters in long-range-ordered films behave in some ways like ferroic domain walls¹⁴ under the constraint of pinning forces due to the existing quenched random electric fields. A small driving ac electric field (approximately close to the threshold field in the

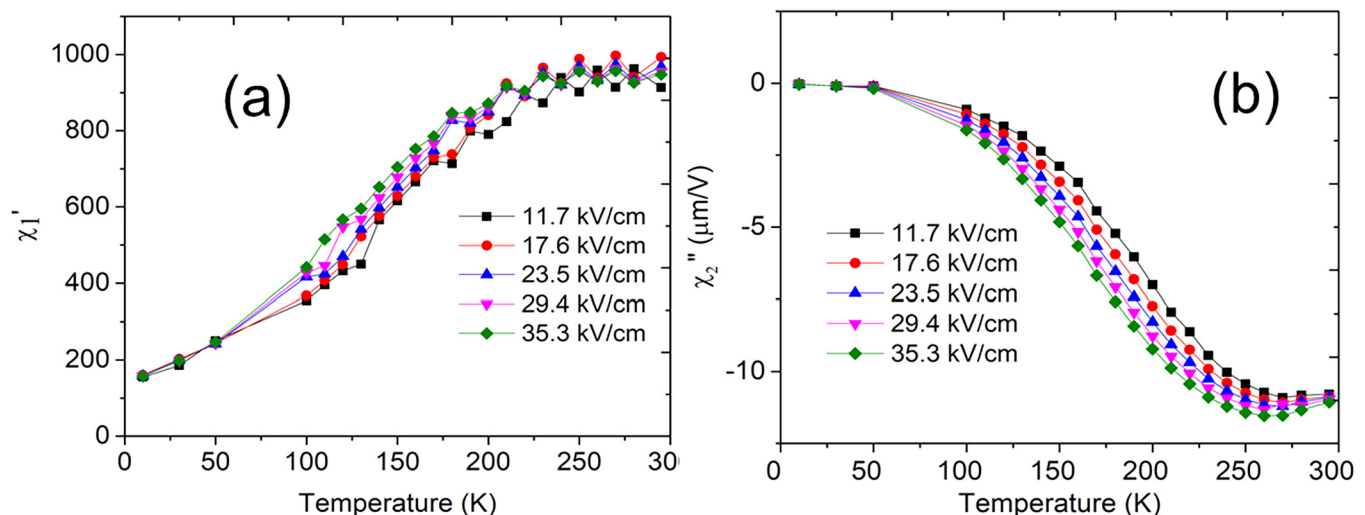


FIG. 6. Temperature dependence of (a) the real part of first- and (b) the imaginary part of second-order susceptibility for short-range-ordered PMN films as a function of electric field (11.7–35.3 kV/cm) measured during a heating cycle.

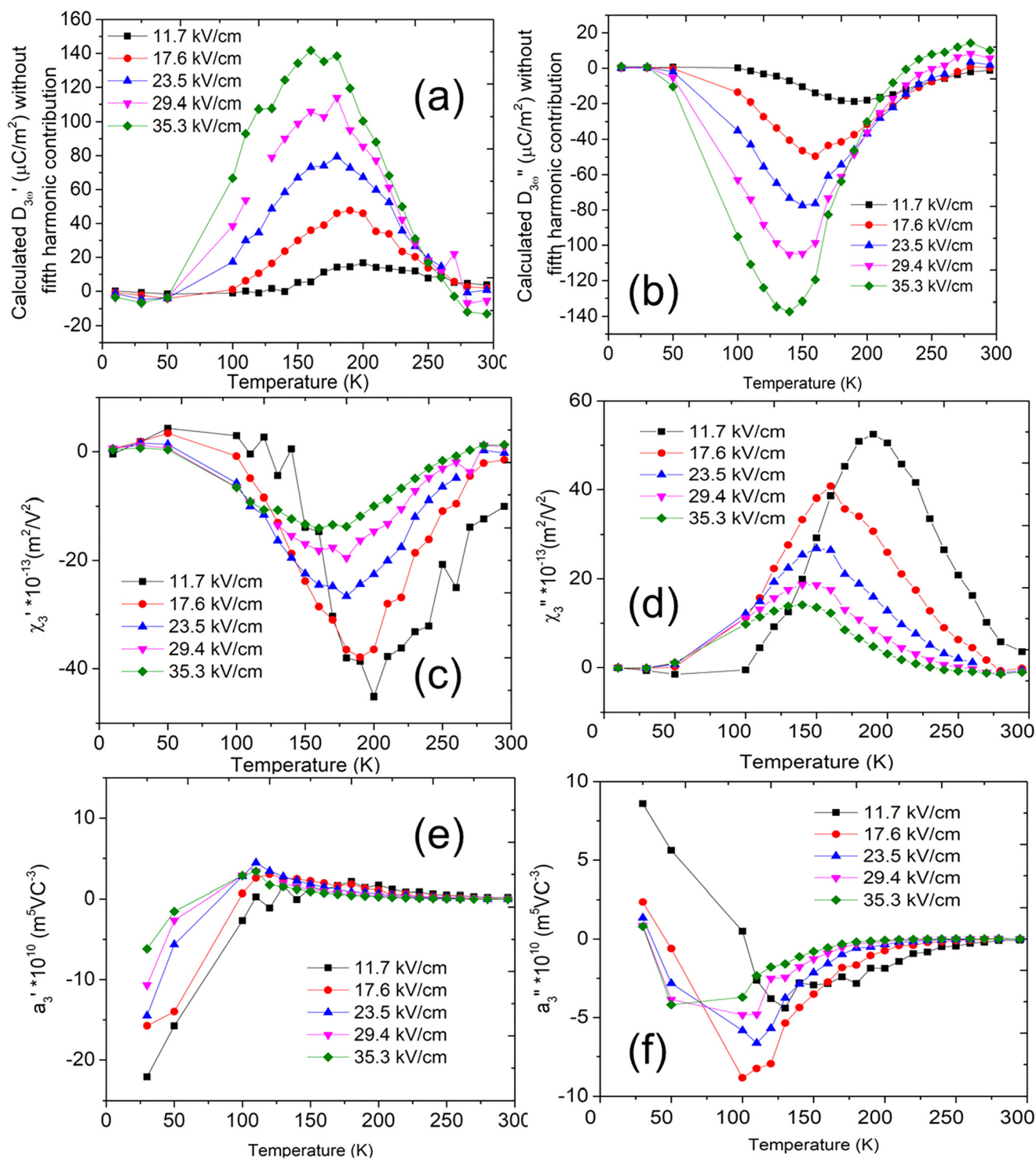


FIG. 7. Temperature dependence of (a) the real part and (b) the imaginary part of third-harmonic dielectric charge displacement without fifth-harmonic contributions, (c) the real part and (d) the imaginary part of third-harmonic susceptibility, (e) scaled-susceptibility parameter a_3' considering real part χ_3' , and (f) scaled-susceptibility parameter a_3'' for short-range-ordered PMN films as a function of electric field (11.7–35.3 kV/cm) measured during a heating cycle.

Rayleigh regime where the third-harmonic phase angle is close to 90°) can overcome the fluctuations of the quenched random field, enabling percolation of frozen polar nanoregions into a more ferroelectric-like state with hysteretic motion of the resulting mobile cluster boundaries.^{14,17} Hence, there is an increase in the hysteretic contributions with decreasing temperature between ~ 240 K and 150 K before dropping as mobile boundaries are gradually frozen out of the system. Unlike the real part of χ_1 , $D_{3\omega}$ is more negative at high ac electric fields, suggesting that domain wall-like contributions could be responsible for the sign change. Additionally, as seen in Fig. 5(d), the temperature where χ_3 has its largest negative magnitude corresponds well with the temperature at which the irreversible Rayleigh coefficient α has its maximum value, and is consistent with a transition from a non-hysteretic to hysteretic behavior with lowering temperatures as reported elsewhere.¹ These observations suggest that in the measured temperature range, the nonlinear properties are more ferroelectric-like at low temperatures ($T \sim 150$ K) and relaxor-like ferroelectrics at higher temperature ($240 \text{ K} < T < 298 \text{ K}$) as a function of the electric field.

In Fig. 5(e), over most of the observed temperature range, a_3 is small and positive. On cooling, it becomes increasingly positive. However, at lower temperatures, a_3 becomes negative and decreases with increasing electric field. On the other hand, the scaled parameter a_3'' calculated using the imaginary part χ_3'' [Fig. 5(f)] diverges around ~ 250 K while peaking at 130 K at the lowest field. This peak shifts with the increasing ac field toward lower temperature. It is notable that temperature-dependent Cole-Cole plots by Kleemann *et al.* suggest pre-transitional freezing of polarization (due to local fluctuations in PNRs) at 240 K, before they coalesce into the ferroelectric phase.¹⁴ However, a peak in a_3 (also predicted by the spherical random-bond random-field model) was not observed in the vicinity of the pre-transitional freezing T_g .

To compare to the long-range-ordered films, Figs. 6(a) and 6(b) and Figs. 7(a)–7(e) show the real part of first-harmonic

and imaginary part of second-harmonic susceptibility, third-harmonic dielectric charge displacement without fifth-harmonic contributions, corresponding to third-harmonic susceptibility and the scaled parameters a_3 and a_3'' as a function of temperature, measured at 1 kHz for the short-range-ordered PMN thin films. While the magnitudes of χ_1' are comparable for the short- and long-range-ordered films, the nonlinearity of the real and imaginary parts of χ_3 [Figs. 7(c) and 7(d)] observed in the short-range-ordered films is slightly higher than that of the long-range-ordered films. This is presumably a consequence of the higher degree of relaxor character in the short-range-ordered films. If the origin of this is Rayleigh-like responses due to polar-cluster boundaries, then there is contribution to both χ_3' and the irreversible Rayleigh coefficient α . Also, like long-range-ordered films, at the lowest measured field, χ_3' remains negative at temperatures greater than 100 K, which is consistent with SRBRF for PMN ceramics.¹⁹ It is expected that, compared to the long-range-ordered films, the short-range-ordered films have larger inherent quenched random field due to higher degree of disorder and require larger fields to achieve percolation. However, this was not observed in the measured range of electric fields. Interestingly, as seen in Figs. 7(e) and 7(f), the variation in real and imaginary parts of a_3 is higher than long-range-ordered films, as it begins to diverge at lower temperature. This might be attributed in part to the loss of ordering due to polar nanoregions in the short-range-ordered films.

Figure 8 shows the summary of the dielectric, SHG, and third-harmonic susceptibility phase for a long-range-ordered PMN film. This suggests that around ~ 150 K, the long-range-ordered film behaves more like a normal ferroelectric. However, with increasing temperature above 240 K, the relaxor character dominates due to the loss of long-range ordering. As a function of temperature, the phase angle of χ_3 moves from showing hysteretic (near -90°) to an-hysteretic behavior (near -180°) behavior. As expected, the phase angle of the third harmonic of polarization, as a function of temperature, shows a dependence on the applied electric field.

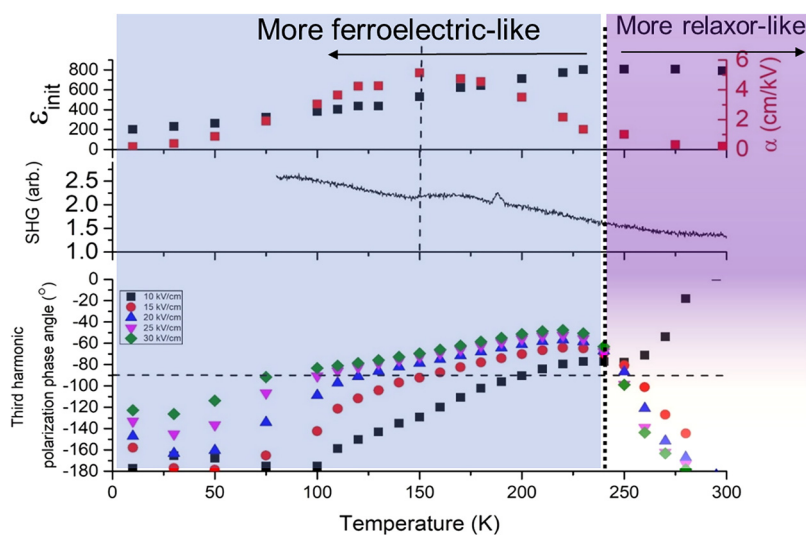


FIG. 8. Summary of nonlinearity data from (a) Rayleigh,¹ (b) second-harmonic generation intensity from (Ref. 1), and (c) third-harmonic polarization phase angle as a function of temperature and electric field for long-range-ordered PMN.

IV. CONCLUSIONS

The dynamic nonlinear dielectric responses of (111)-oriented $\text{PbMg}_{1/3}\text{Nb}_{2/3}\text{O}_3$ were studied as a function of temperature for thin films with long- and short-range ordering. The ordering achieved during the synthesis of the long-range-ordered film was insufficient to achieve a fully normal ferroelectric state. Below 240 K, these films required a small ac field to overcome the quenched random electric and facilitate percolation of the polar nano-region. The boundaries of these clusters behaved hysterically in accordance to the Rayleigh law, thus acting more like a normal ferroelectric at lower temperature ($T \sim 150$ K). The films behave like a typical relaxor ferroelectric near room temperature. With reduced ordering, the short-range-ordered films exhibit greater dispersion in linear and higher order harmonic dielectric charge displacement density.

ACKNOWLEDGMENTS

This work was funded by the Penn State MRSEC, Center for Nanoscale Science, under Award No. NSF DMR-1420620. The authors would also like to acknowledge the help of Jeff Long in electrical characterization setup. L. W. Martin acknowledges support from the National Science Foundation (NSF) under Grant No. DMR-1708615.

DATA AVAILABILITY

The data that support the findings of this study are available within the article.

REFERENCES

- ¹S. Shetty, A. Damodaran, K. Wang, Y. Yakun, V. Gopalan, L. Martin, and S. Trolier-McKinstry, *Adv. Funct. Mater.* **29**, 1804258 (2019).
- ²D. V. Taylor and D. Damjanovic, *Appl. Phys. Lett.* **73**, 2045 (1998).
- ³D. V. Taylor and D. Damjanovic, *J. Appl. Phys.* **82**, 1973 (1997).
- ⁴N. Bassiri-Gharb, I. Fujii, E. Hong, S. Trolier-McKinstry, D. V. Taylor, and D. Damjanovic, *J. Electroceramics* **19**, 49 (2007).
- ⁵S. Trolier-McKinstry, N. Bassiri Gharb, and D. Damjanovic, *Appl. Phys. Lett.* **88**, 202901 (2006).
- ⁶S. Li, W. Cao, and L. E. Cross, *J. Appl. Phys.* **69**, 7219 (1991).
- ⁷V. Bobnar, Z. Kutnjak, R. Pirc, R. Blinc, and A. Levstik, *Phys. Rev. Lett.* **84**, 5892 (2000).
- ⁸W. Kleemann, S. Miga, J. Dec, and J. Zhai, *Appl. Phys. Lett.* **102**, 232907 (2013).
- ⁹J. Dec, S. Miga, W. Kleemann, and B. Dkhil, *Ferroelectrics* **363**, 141 (2008).
- ¹⁰J. Dec, S. Miga, and W. Kleemann, *Ferroelectrics* **417**, 82 (2017).
- ¹¹D. Damjanovic, *Hysteresis in Piezoelectric and Ferroelectric Materials* (Academic Press, 2006).
- ¹²S. Hashemizadeh and D. Damjanovic, *Appl. Phys. Lett.* **110**, 192905 (2017).
- ¹³A. E. Glazounov and A. K. Tagantsev, *J. Phys. Condens. Matter* **10**, 8863 (1998).
- ¹⁴W. Kleemann and J. Dec, *Phys. Rev. B* **94**, 174203 (2016).
- ¹⁵V. Westphal, W. Kleemann, and M. D. Glinchuk, *Phys. Rev. Lett.* **68**, 847 (1992).
- ¹⁶W. Kleemann and J. Dec, *Ferroelectrics* **553**, 1 (2019).
- ¹⁷D. Fu, H. Taniguchi, M. Itoh, S. Y. Koshihara, N. Yamamoto, and S. Mori, *Phys. Rev. Lett.* **103**, 207601 (2009).
- ¹⁸A. Koreeda, H. Taniguchi, S. Saikan, and M. Itoh, *Phys. Rev. Lett.* **109**, 197601 (2012).
- ¹⁹R. Pirc and R. Blinc, *Phys. Rev. B* **60**, 13470 (1999).
- ²⁰R. Pirc, R. Blinc, and V. Bobnar, *Phys. Rev. B* **63**, 054203 (2001).
- ²¹A. Glazounov and A. K. Tagantsev, *Phys. Rev. Lett.* **85**, 2192 (2000).
- ²²R. Pirc, R. Blinc, and Z. Kutnjak, *Phys. Rev. B* **65**, 214101 (2002).
- ²³Z. G. Ye, *Key Eng. Mater.* **155–156**, 81 (1998).
- ²⁴S. S. N. Bharadwaja, E. Hong, S. J. Zhang, L. E. Cross, and S. Trolier-McKinstry, *J. Appl. Phys.* **101**, 104102 (2007).
- ²⁵J. Dec, W. Kleemann, S. Miga, C. Filipic, A. Levstik, R. Pirc, T. Granzow, and R. Pankrath, *Phys. Rev. B* **68**, 092105 (2003).
- ²⁶W. Kleemann, *J. Mater. Sci.* **41**, 129 (2006).
- ²⁷S. Miga, J. Dec, and W. Kleemann, *Ferroelectrics: Characterization and Modeling*, edited by M. Lallart (IntechOpen, 2011), p. 181.
- ²⁸M. Tyunina, J. Levoska, K. Kundzinsh, and V. Zauls, *Phys. Rev. B* **69**, 224101 (2004).